

# On the 2015 St. Patrick Storm Turbulent State of the Ionosphere: Hints from the Swarm Mission

P. De Michelis<sup>1</sup>, A. Pignalberi<sup>1</sup>, G. Consolini<sup>2</sup>, I. Coco<sup>1</sup>, R. Tozzi<sup>1</sup>, M. Pezzopane<sup>1</sup>, F. Giannattasio<sup>1</sup>, and G. Balasis<sup>3</sup>

<sup>1</sup>Istituto Nazionale di Geofisica e Vulcanologia, 00143 Rome, Italy

<sup>2</sup>INAF-Istituto di Astrofisica e Planetologia Spaziali, 00133 Rome, Italy

<sup>3</sup>IAASARS-National Observatory of Athens, Athens, Greece

## Key Points:

- Self-similarity/affinity nature of the plasma density fluctuations in the F region of mid- and high-latitude ionosphere
- Plasma density fluctuations at high latitudes in the auroral and polar cap regions seem to be related to a turbulent ionospheric dynamics
- High values of RODI can be a proxy of the occurrence of ionospheric turbulence

## Plain Language Summary

Electron density fluctuations characterizing the ionospheric plasma during the St. Patrick's geomagnetic storm occurred on 17 March 2015 are analyzed to investigate their possible turbulent nature. To perform this study electron density values recorded by two of the three satellites of the Swarm constellation are considered at mid and high latitudes of both hemispheres between 16 and 22 March 2015. Results show that electron density fluctuations present interesting patterns and that high values of the Rate Of change of electron Density Index (RODI), which is used as an ionospheric disturbance index, may be related to a turbulent dynamics of the ionosphere. Specifically, independently of the different phases of the analyzed geomagnetic storm the observed features seem to support the idea of a fluid and/or magnetohydrodynamic turbulence as the main cause of the high values of RODI recorded at high latitudes in the auroral and polar cap regions.

---

Corresponding author: Paola De Michelis, [paola.demichelis@ingv.it](mailto:paola.demichelis@ingv.it)

This article has been accepted for publication and undergone full peer review but has not been through the copyediting, typesetting, pagination and proofreading process which may lead to differences between this version and the Version of Record. Please cite this article as doi: [10.1029/2020JA027934](https://doi.org/10.1029/2020JA027934)

## Abstract

The scaling features of electron density fluctuations during the St. Patrick's magnetic storm (17 March 2015) are analyzed to try to characterize the possible turbulent nature of the ionosphere during the development of the geomagnetic storm. The electron density values recorded by two of the three satellites of Swarm constellation during a period of 7 days (16-22 March 2015) around the storm peak are analyzed at mid- and high-latitude regions in both hemispheres. The analysis reveals interesting patterns in the scaling properties of electron density fluctuations and a possible explanation for the occurrence of high values of the Rate of change Of the electron Density Index (RODI). Indeed, the obtained results seem to suggest that very high values of RODI, which describes the structuring of the plasma within a fixed time and is used as an ionospheric disturbance index, are correlated with the antipersistent character of electron density fluctuations and with the values around  $5/3$  of the power spectral density scaling exponent. These features are independent of the different phases of the analyzed geomagnetic storm and seem to support the idea of a fluid and/or magnetohydrodynamic turbulence as the main responsible of the high values of RODI recorded at high latitudes in the auroral and polar cap regions.

## 1 Introduction

Turbulence phenomena are at the origin of several important ionospheric dynamical processes. They usually happen as a result of the coupling processes which characterize the solar wind-magnetosphere-ionosphere system and can significantly affect both the ionospheric plasma dynamics and the energization of ionospheric particles. Consequently, the dynamics of physical quantities like electron and ion densities, velocities and temperatures, and magnetic and electric fields, can display fluctuations occurring on many spatial and temporal scales, among which a nonlinear transfer of energy can occur.

One of the first review papers focusing on the ionospheric plasma turbulence is the one published in the mid-eighties by *Kintner and Seyler* (1985) which proposes and discusses different theories and models on turbulence mechanisms, capable of explaining particular behaviors shown in the ionosphere by both the electron density and the electric field. Beyond this interesting review, it should be stressed, however, that in the years many other papers have been published on the occurrence of turbulence processes in the ionosphere. For example, a great attention has been given to the turbulent properties of electric (see, e.g., *Golovchanskaya and Kozelov*, 2010; *Heppner et al.*, 1993; *Kozelov and Golvchanskaya*, 2006; *Tam et al.*, 2005; *Weimer et al.*, 1985) and magnetic fluctuations (*De Michelis et al.*, 2015; *Golovchanskaya et al.*, 2006; *Kozelov and Golvchanskaya*, 2006) observed at different altitudes and latitudes by ground and space. The increased interest in the ionospheric turbulence phenomena (e.g., *De Michelis et al.*, 2017; *Dyrud et al.*, 2008; *Grach et al.*, 2016; *Pécseli*, 2016; *Spicher et al.*, 2015) demonstrates the need to better understand these processes and the different ways in which they can influence the ionospheric environment. For instance, the generation and dynamics of ionospheric inhomogeneities and irregularities (see, e.g., *Basu et al.*, 1988; *Earle et al.*, 1989; *Gian-nattasio et al.*, 2019) can be affected by turbulence processes occurring in the plasma and this means that ionospheric turbulence may play a significant role in the framework of space weather. Indeed, the ionospheric inhomogeneities and irregularities are among the main causes of disturbances in the propagation of electromagnetic signals in the ionosphere and consequently a better understanding of the turbulence will be of help to all those systems, such as the Global Positioning Systems (GPS) and Global Navigation Satellite Systems (GNSS) which are based on the propagation of an electromagnetic signals through the ionosphere.

Ionosondes, incoherent scatter radars, VHF/HF coherent backscatter radars, all-sky cameras, and GPS stations are usually used to investigate ionospheric irregularities.

77 However, these ground-based measuring facilities, which permit a good investigation of  
78 irregularities in the bottomside of the ionosphere, do not permit a good investigation of  
79 the topside ionospheric irregularities where in situ observations can be more useful. These  
80 can be obtained using instruments on-board of low-Earth-orbit (LEO) satellites. Thus,  
81 a good opportunity to unveil how turbulence affects the ionospheric environment, in gen-  
82 erating multi-scale plasma structures and plasma inhomogeneities, comes from the anal-  
83 ysis of the nature of fluctuations and their multi-scaling features of the electron density  
84 estimated by data as recorded by the European Space Agency (ESA) Swarm mission.

85 The Swarm constellation was launched in November 2013 to provide high-quality  
86 measurements of Earth's magnetic field and associated plasma environment (*Olsen et*  
87 *al.*, 2013). These three identical satellites, which fly in polar orbit at two different alti-  
88 tudes of about 450 km (Swarm A and Swarm C) and 510 km (Swarm B), explore the  
89 F region of the ionosphere through the measurements of a vector fluxgate, an absolute  
90 scalar magnetometers and the Electric Field Instrument (EFI), which includes Langmuir  
91 Probes (LPs) and a Thermal Ion Imager for measuring plasma density and temperature  
92 (*Knudsen et al.*, 2017).

93 It is evident that data recorded on-board LEO satellites give the opportunity to  
94 study the ionospheric irregularities at different latitudinal regions. Here, we focus on mid-  
95 and high-latitude regions of both hemispheres. Indeed, while for the equatorial regions  
96 there have been a number of experimental studies accompanied with analytical models  
97 (*Kelley*, 2009), there has been a much slower progress about studies of the high-latitude  
98 ionospheric plasma irregularities associated with instabilities and turbulence. This is in  
99 part due to difficult accessibility of these regions and to the complex dynamics of the iono-  
100 spheric plasma at high latitudes.

101 Among some recent papers on high-latitude plasma density irregularities, *Spicher*  
102 *et al.* (2015) have clearly shown how nonlinear wave interactions and coherent mode cou-  
103 pling might play a relevant role in generating electron density fluctuations at the edge  
104 of the polar cap, while in the region where electron precipitation is dominant, the fluc-  
105 tuations associated with a plasma enhancement are mainly characterized by a more ran-  
106 dom nature. All these findings suggest that a clear link between particle precipitation  
107 and turbulent-like structures exists in these regions. To analyze the ionospheric plasma  
108 irregularities and turbulence a common approach is to study the power spectra of the  
109 electron density responsible for these irregularities and, in particular, their slopes which  
110 could give information on the possible mechanism through which these irregularities are  
111 generated. In the high-latitude F region the analysis of the power spectra of plasma den-  
112 sity fluctuations in the range of scales between several kilometers and tens of meters shows  
113 that spectra are often characterized by a power law with a spectral index around  $-1.8$   
114 (e.g., *Basu et al.*, 1984; *Dyson et al.*, 1974; *Mounir et al.*, 1991). This suggests that the  
115 generation of plasma irregularities in the ionospheric polar regions could be associated  
116 with the gradient drift instability (e.g., *Cerisier et al.*, 1985; *Mounir et al.*, 1991) or with  
117 the Kelvin-Helmholtz instability (*Basu et al.*, 1988; *Kintner and Seyler*, 1985).

118 In this work data recorded on-board Swarm satellites are used to get information  
119 about the turbulent nature of the ionospheric plasma at mid and high latitudes in both  
120 hemispheres by analyzing the scaling features of small-scale fluctuations of the electron  
121 density recorded during the St. Patrick's geomagnetic storm of March 2015, the well-  
122 known St. Patrick's event. It was the strongest geomagnetic storm of the 24th solar cy-  
123 cle that reached the G4 level on the NOAA scale (*Poppe*, 2000). It was characterized by  
124 an intense particle precipitation in the polar regions that generated both an enhance-  
125 ment in substorm activity and the occurrence of intense ionospheric irregularities dur-  
126 ing the main and recovery phases of the geomagnetic storm (*Cherniak et al.*, 2015). This  
127 geomagnetic storm has been extensively investigated in the scientific community, for ex-  
128 ample analyzing the ionospheric effects on global scale (*Astafyeva et al.*, 2015), on the  
129 equatorial latitudes of the Indian and nearby regions (*Ram et al.*, 2015; *Ramsingh et al.*,

130 2015), on middle and low latitudes (*Balasis et al.*, 2018; *Nava et al.*, 2016). We analyze  
131 this event from a completely different point of view. The main aims are indeed: 1) to  
132 analyze the daily patterns of the scaling properties of electron density fluctuations dur-  
133 ing the development of this geomagnetic storm, 2) to investigate a possible relation be-  
134 tween them and the occurrence of plasma density irregularities as described by the Rate  
135 Of change of electron Density Index (the so-called RODI) (*Jin et al.*, 2019). The main  
136 idea proposed by this work is to try to understand if there is a correlation between RODI  
137 and the scaling/spectral features of electron density fluctuations and so if RODI can be  
138 used as a proxy for the occurrence of ionospheric plasma turbulence.

139 Indeed, RODI obtained by measurements made on-board Swarm constellation, is  
140 a measure of the occurrence of irregularities at the Swarm altitude. So, it would be po-  
141 tentially able to give us information about the nature of ionospheric irregularities achieved  
142 at the same altitude. This would give a additional importance to an index, well known  
143 and used in the scientific community, born as a simple measure of the electron density  
144 irregularities and able to identify their presence but not their nature.

## 145 2 Data and processing approach

146 The present work focuses on the analysis of the fluctuations of in-situ electron den-  
147 sity provided by the LPs on-board Swarm satellites during the geomagnetic storm oc-  
148 curred on 17 March 2015. Level 1b electron density data at a rate of 1 Hz for two of the  
149 three Swarm satellites (A and B) have been selected from the ESA ftp repository ([https :  
150 //earth.esa.int/web/guest/swarm/data-access](https://earth.esa.int/web/guest/swarm/data-access)) for a time window of seven days from  
151 16 to 22 March 2015. According to the "Swarm Level 1b Product Definition" document  
152 (available at [https :  
153 //earth.esa.int/web/guest/document-library/browse-document-  
154 library/-/article/swarm-level-1b-product-definition](https://earth.esa.int/web/guest/document-library/browse-document-library/-/article/swarm-level-1b-product-definition)), we have excluded data  
155 flagged as "non nominal" (parameters `Flags_Ne` and `Flags_Te` different from either 10  
156 or 20). Then, all data gaps resulting either from flag selection or from data unavailabil-  
157 ity have been filled by "not-a-number" values, in order to guarantee the continuity of  
the time series.

158 Data are presented in terms of Quasi-Dipole (QD) latitude (*Laundal and Richmond*,  
159 2016) and magnetic local time (MLT) coordinates and reported in polar view daily maps  
160 in both hemispheres (from  $50^\circ$  to the magnetic pole). In each map, magnetic noon is at  
161 the top and magnetic midnight is at the bottom.

162 Figure 1 shows polar daily maps of the electron density for the Northern Hemisphere  
163 covering the selected time interval. These maps, obtained considering the measurements  
164 coming from Swarm A and Swarm B, are reported together with the temporal trend of  
165 two different geomagnetic indices, SYM-H and AE, which well describe the geomagnetic  
166 activity in the mid- and high-latitude regions during the selected period. These indices  
167 allow to following the temporal evolution of the disturbance of the geomagnetic field recorded  
168 on the ground mainly due to: an increase of the magnetospheric ring current, an intense  
169 particle precipitation at high latitudes which cause a substorm activity enhancement.  
170 Due to orbital features, during the analyzed period Swarm A and B span two different  
171 magnetic local time intervals (06:00-09:00 MLT and 18:00-21:00 MLT, respectively) as  
172 it is evident in Figure 1. The same data daily polar maps are drawn for the case of the  
173 Southern Hemisphere in Figure 2. The comparison between Figure 1 and 2 shows the  
174 different spatial extent of data in the two hemispheres, which is due to the different dis-  
175 tance of the magnetic poles from the geographic ones. Polar daily maps of electron den-  
176 sity show a well-known feature characterizing disturbed conditions, that is a significant  
177 electron density decrease due to compositional changes (*Prölss*, 1987).

178 The in situ electron density data have been used to evaluate RODI, which is the  
179 standard deviation of the Rate of change Of electron Density (ROD) in a sliding win-

180 dow of fixed size. This index has been evaluated according to *Jin et al. (2019)* and con-  
 181 sidering a sliding window of 10 s. RODI polar daily maps in QD latitude versus MLT  
 182 coordinates are also reported in Figure 1 and Figure 2 for the Northern and Southern  
 183 Hemisphere respectively. From a preliminary inspection of RODI spatial distributions  
 184 we may note how the higher values of RODI ( $> 3 \times 10^3 \text{ cm}^{-3}\text{s}^{-1}$ ) are mainly located  
 185 in the polar cap roughly along the Noon-Midnight sectors, while the auroral oval region  
 186 seems to be associated with values of RODI  $< 3 \times 10^3 \text{ cm}^{-3}\text{s}^{-1}$ . This could be a rele-  
 187 vant aspect to be compared with the average scaling features in the two regions. We will  
 188 return on this point later in the next Sections.

189 By comparing Figures 1 and 2 no important North-South asymmetry is visible: nei-  
 190 ther in electron density and RODI patterns nor in their temporal evolution during the  
 191 geomagnetic storm. The only differences are in the intensity of the variation of electron  
 192 density and RODI that is slightly more intense in the Southern Hemisphere than in the  
 193 Northern one, and in a partial different location of the higher RODI values on 17 March.  
 194 We notice that in both hemispheres the period of the most intense irregularity occur-  
 195 rence corresponds with the main phase of the geomagnetic storm (occurred on 17 March  
 196 2015) when the position of the irregularities is within an oval around  $60^\circ$  QD-Lat. That  
 197 is clearly visible in the Southern Hemisphere. During the recovery phase of the storm  
 198 the region characterized by the occurrence of irregularities tends to shrink in both hemi-  
 199 spheres. Indeed, the equatorward expansion of zone characterized by irregularity stops  
 200 with the beginning of the recovery phase of the storm when the high values of RODI are  
 201 mainly confined in an oval within  $65^\circ$ – $70^\circ$  QD-Lat. An interesting signature of the ir-  
 202 regularity pattern can be recognized in both hemispheres, that is the strongest and most  
 203 pronounced irregularities, i.e. the highest values of RODI, are oriented in the day–night  
 204 direction across the polar cap. The irregularities along this direction are stronger than  
 205 those occurring along the auroral border. This means that the gradients of the ionospheric  
 206 electron density induced by this geomagnetic storm were related both to auroral parti-  
 207 cle precipitation (on the auroral border) and to plasma large scale convective motions  
 208 (in the day-night direction). Indeed, the radial structure of the ionospheric irregulari-  
 209 ties have been associated mainly with the convection pattern anti-sunward across the  
 210 polar cap of the electron density gradients (*Cherniak et al., 2015; Cherniak and Zakharenkova,*  
 211 *2016*) and not to the auroral particle precipitation.

### 212 3 Data Analysis

213 To investigate the scaling features of the electron density fluctuations we investi-  
 214 gate the self-similarity/affinity nature of the measured time series using the  $q^{\text{th}}$ -order  
 215 structure function  $S_q(\ell)$  for different scales ( $\ell$ ). This method consists in evaluating the  
 216 scaling features of the moments of the signal increments at different spatial scales. Here,  
 217 we computed the so-called generalized structure functions of the electron density that  
 218 means to compute the  $q^{\text{th}}$ -order structure functions as a function of the time-delay  $\tau$ ,  
 219 i.e.,

$$220 S_q(\tau) = \langle |N_e(t + \tau) - N_e(t)|^q \rangle, \quad (1)$$

221 where  $N_e$  is the electron density,  $t$  is the time,  $\tau$  is the time-delay and  $\langle \dots \rangle$  stands for a  
 statistical average. For a scaling process, a power-law behavior is expected, i.e.,

$$222 S_q(\tau) = \tau^{\xi(q)}, \quad (2)$$

223 where  $\xi(q)$  are the scaling exponents of the structure functions. In the case of simple frac-  
 224 tal signals these exponents are expected to be a linear function of the moment order  $q$ ,  
 225 while in the case of more complex fractal signals they show a departure from such a lin-  
 ear dependence.

Among the hierarchy of scaling exponents  $\xi(q)$  the scaling exponents of order  $q = 1$  and  $2$  can be very useful to quantify some specific features of the signal under investigation. The first-order scaling exponent  $\xi(1)$ , also known as *Hurst/Hölder exponent*  $H$  (*Hurst*, 1956), quantifies the self-affine features of the signal and, in particular, the persistence or antipersistent character of the increments.  $H$  is a measure of the signal “roughness”. A signal, whose scaling features are characterized by a Hurst exponent value less than  $0.5$  ( $H < 0.5$ ), shows an antipersistent character of its increments (a higher roughness than a random Gaussian Brownian motion), while a signal, whose scaling features are characterized by a Hurst exponent value greater than  $0.5$  ( $H > 0.5$ ), shows a persistent character of its increments (*Balasis et al.*, 2006). In other words, long-range correlated signals are characterized by a sign-persistence of its increments ( $H > 0.5$ ), while in the case of antipersistent increments ( $H < 0.5$ ) we talk about short-range correlated signals. Furthermore, the second-order scaling exponent  $\xi(2)$  is capable of providing an information on the signal spectral features via the Wiener-Khinchin theorem (*Wiener*, 1964). It links the spectral features to the Fourier transform of the auto-correlation function, to which the second-order structure function is directly related. In particular, in the case of a temporal signal  $f(t)$  displaying scaling features characterized by a scaling exponent  $\xi(2)$  for the second-order structure function, the power spectral density (PSD) is expected to satisfy the following power-law:

$$PSD(f) \sim f^{-\beta}, \quad (3)$$

where

$$\beta = \xi(2) + 1. \quad (4)$$

Thus, the investigation of scaling features of the second-order structure function can provide information on the spectral features. In passing, we note that in the case of a homogeneous fractal signal the second-order scaling exponent,  $\xi(2)$ , is linearly related to the first one, i.e.,  $\xi(2) = c \xi(1)$ , being  $c$  a constant. Deviation from this linear scaling can be associated with the occurrence of anomalous scaling features, i.e., with a multifractal structure of the signal increments.

The study of scaling features may require to adopt some precautions in the case of real signals for which it is not possible to assume that some specific conditions are satisfied. Indeed, while for simple mathematical signals the scaling features are generally global, for real signals these properties can acquire a local character due to their inherent spatio-temporal nonstationarity. This is what happens in the case of satellite observations because satellites cross different regions observing physical situations that can change in space and time. To approach the study of these kind of observations, it is necessary to find reliable methods capable of evaluating the local scaling features in the different regions explored by satellites along their orbits and under different geomagnetic and interplanetary conditions. The very irregular character of the original Swarm data, which is a consequence of the strong inhomogeneity of the ionospheric plasma regions crossed by the satellites, suggests to use a local structure function method to compute their scaling features from signal increments (see, e.g., *De Michelis et al.*, 2015, and references therein). Indeed, in this case, methods based on detrending approaches and fluctuation field analyses (*Alessio et al.*, 2002; *Carbone et al.*, 2004; *Peng et al.*, 1994) could turn out to be inadequate, providing controversial results which are strongly dependent on the detrending procedure. This has been tested over a wide set of surrogated fractional, fractal and multifractional time series, which evidenced how to our purposes the use of a local structure function method returns the best results in terms of local estimation (error less than 10%).

The structure function analysis is commonly used to analyze turbulent fields on a global scale so that, in order to apply this method locally, we need to implement it on

274 overlapping moving windows and to remove possible large-scale variations that can af-  
 275 fect a correct estimation of the scaling features. This is the approach of the detrended  
 276 structure function analysis proposed by *De Michelis et al.* (2015). This method is based  
 277 on three steps. Let  $f(t)$  be a time series evenly sampled at fixed time intervals and  $f_N(t)$   
 278 a portion of it falling in a window whose size is of  $N$  points. The first step of the method  
 279 consists in locally detrending the  $f_N(t)$  portion of the signal by using a polynomial func-  
 280 tion  $p_N^k(t)$  of order  $k$ , defining a detrended function  $g_N(t)$  as:

$$g_N(t) = f_N(t) - p_N^k(t). \quad (5)$$

281 The polynomial function is estimated by means of the traditional least-squared method.  
 282 As a second step, the usual structure function analysis is applied, i.e., the scaling fea-  
 283 tures are computed studying the scaling properties of the  $q^{\text{th}}$  order structure function,  
 284  $S_q(\tau)$ , defined on the detrended function  $g_N(t)$ , as follows:

$$S_q(\tau) = \langle |g_N(t + \tau) - g_N(t)|^q \rangle \sim \tau^{\xi(q)}. \quad (6)$$

285 Here  $\xi(q)$  are the scaling exponents, where  $\xi(1) \equiv H$ . The maximum moment order  $q_m$   
 286 that can be locally evaluated depends on the size of the moving window which should  
 287 be at least of  $10^{q_m}$  points, being  $q_m$  the maximum moment order. Regarding the choice  
 288 of the degree  $k$  of the polynomial used to locally detrend the times series we simply re-  
 289 move a linear trend on the selected time window.

290 The third step consists in defining the dimension of the moving window. Gener-  
 291 ally, a good window size is such that  $N$  is at least one order of magnitude larger than  
 292 the number of points corresponding to the maximum scale to investigate. Recalling that  
 293 we are using 1 Hz data, this means that if we want to study the scaling features in a range  
 294 of scales from 1 s up to  $\tau$ , the expected number of points that define the width of the  
 295 moving window should be of the order of  $N \sim 10\tau$ . In our case, we consider  $N = 301$   
 296 that means a moving window of 301 s. Detrended structure function analysis is applied  
 297 in this window that is then shifted of 1 point, i.e. 1 s. An accurate error analysis on sur-  
 298 rogated data has clearly shown that error on local estimation of the scaling exponents  
 299 is  $\leq 10\%$ . The time scales ( $\tau$ ) between 1 s and 40 s are analyzed and the estimated val-  
 300 ues of the first and second scaling exponents are associated with the position of the satel-  
 301 lite in the instant of time that corresponds to the center of the considered time window.  
 302 We suppose that the results obtained in the time domain are also valid in the spatial one.  
 303 The idea is that the temporal scales can be related to the spatial scales and consequently,  
 304 taking into account the orbital velocity of Swarm satellite ( $\sim 7.6$  km/s), the range of  
 305 fluctuation scales  $\tau$  corresponds to the range of spatial fluctuations between  $\sim 8$  km and  
 306  $\sim 250$  km. This hypothesis is based on the fact that the observed low frequency tem-  
 307 poral electron density fluctuations in the satellite reference frame are dominated primar-  
 308 ily by Doppler-shifted, and essentially stationary, spatial variations of the electron den-  
 309 sity structures. Thus, the time scale  $\tau$  and frequency  $f$  may be viewed essentially as spa-  
 310 tial scale  $\delta \sim v_{\text{sp}}\tau$  and mode number  $k \sim 2\pi f/v_{\text{sp}}$  with  $v_{\text{sp}}$  being the spacecraft ve-  
 311 locity (e.g., *Chaston et al.*, 2008; *Kintner and Seyler*, 1985, and references therein). On  
 312 the other hand, the range of investigated timescales (from 1 s up to 40 s) includes time  
 313 intervals where it can be reasonably assumed that the structures are mainly frozen, as  
 314 also reported in some previous papers (e.g. *De Michelis et al.*, 2017; *Gjerloev et al.*, 2011),  
 315 where it was clearly shown that in the dayside/nightside sectors structures are nearly  
 316 stable up to 60/160 s, respectively.

317 To limit a considerable loss of points as the consequence of the moving window ap-  
 318 proach, we analyze a single time series (electron density values) of 604800 (number of  
 319 values recorded per day (86400) multiplied by the number of considered day (7)) points  
 320 for each satellite, so the new time series relative to the first and second scaling exponents  
 321 have only 300 points less than the original one. Clearly, data refer to the entire globe

and to the entire time interval, therefore a selection of the values in the areas of interest, as well as for the day of interest, is necessary. For this reason, the entire time series of the selected time interval is divided into daily subsets and for each subset the first and second scaling exponents values obtained considering Swarm A and B observations during their crossings of the Northern and Southern Hemisphere are considered, simultaneously. At the end of this process we obtain 30 crossings (15 crossings per day per each satellite) for each hemisphere. Daily maps are then drawn by reducing data on a regular grid using a Gaussian kernel interpolation scheme.

## 4 Results

Figure 3 reports the results obtained for the Northern Hemisphere while those for the Southern Hemisphere are reported in Figure 4. Polar daily maps of both the first and the second scaling exponents for the time interval 16-22 March 2015 are shown together with the polar daily maps of RODI. All these quantities are represented as a function of QD-latitude and magnetic local time. The daily maps of the first-order scaling exponent (Figure 3, first column) in the interval  $[0.2, 0.8]$  give the opportunity to distinguish regions where the electron density fluctuations have a persistent character ( $H > 0.5$  in red) from those characterized by an antipersistent one ( $H < 0.5$  in blue). The antipersistent character seems to be a typical feature of high latitudes ( $> 60^\circ$ ) and the size of the region characterized by this antipersistent nature of the electron density fluctuations appears to increase approaching to and during the main phase of the geomagnetic storm. Conversely, the persistent character appears to be a typical feature of mid latitudes ( $< 60^\circ$ ) where the values of  $H$  are everywhere greater than 0.5 regardless of the geomagnetic activity level. During the temporal evolution of the geomagnetic storm, the main feature is essentially the position of the profile defined by values of  $H$  equal to 0.5, that seems to follow the spatial and temporal evolution of the auroral zone during the selected period. The daily maps relative to the second-order scaling exponent (Figure 3, fifth column) show as the ionospheric polar regions are characterized by different values in the range between 0.5 and 1.8. Generally, the regions with an antipersistent character of the electron density fluctuations are characterized by values of the second order scaling exponent less than 1. This means that the scaling exponent ( $\beta$ ) of the power spectrum of the original signal is less than 2. Conversely, regions characterized by a more persistent behavior are usually associated with values  $\xi(2)$  greater than 1 and consequently with values  $\beta$  greater than 2 at all analyzed scales. This suggests the existence of different scaling features which depend on the latitude, MLT and geomagnetic activity level. Similar results are obtained for the Southern Hemisphere as it is shown in Figure 4.

The ionospheric regions marked by an antipersistent character of the electron density fluctuations and values of the second-order scaling exponent less than 1 seem to correspond to those regions where high values of RODI are recorded (see Figure 3 and Figure 4, central column). To investigate the possible relationship between this index and the scaling features of the electron density fluctuations, the joint probability distributions between RODI and the first (Figure 3 and Figure 4, second column) and second-order scaling exponents (Figure 3 and Figure 4, fourth column) respectively, have been evaluated. High values of RODI are correlated with an antipersistent character ( $H < 0.5$ ) of the electron density fluctuations and values of the second-order scaling exponent  $\xi(2)$  in the range from 0.5 to 0.7 (or  $\beta$  around 1.66). These features remain throughout the entire development of the storm and characterize both hemispheres. Low values of RODI are instead correlated with a persistent character ( $H > 0.5$ ) of the electron density fluctuations and values of second-order scaling exponent  $\xi(2)$  greater than 1 (or  $\beta > 2$ ). The results suggest the existence of two different families of irregularities whose origin must be sought in different physical processes. We notice that the relative weight of the two families changes day after day during the analyzed period. The family of irregularities associated with a persistent character of the electron density fluctuations and



374 values of the second-order scaling exponent greater than 1 becomes particularly visible  
 375 during less disturbed days. It is also possible to notice a slight difference between the  
 376 results obtained in the Northern and Southern Hemisphere. In the Southern Hemisphere  
 377 this family of irregularities shows a greater joint probability with respect to the North-  
 378 ern Hemisphere. Conversely, the family of irregularities associated with an antipersis-  
 379 tent character of the electron density fluctuations and values of the second-order expo-  
 380 nent less than 1 seems to increase in the disturbed period, i.e. during the main phase  
 381 of the geomagnetic storm and the started of the recovery phase.

382 A more careful analysis of these two distinct families of irregularities shows that  
 383 these are actually associated with different values of latitudes. High RODI values ( $> 10^{3.5}$   
 384  $\text{cm}^{-3} \text{s}^{-1}$ ) characterized by electron density fluctuations with an antipersistent behaviour  
 385 and  $\beta$  around 1.66, can be found at high latitudes mainly in the auroral oval; low RODI  
 386 values, characterized by electron density fluctuations with a persistent behavior and  $\beta$   
 387 larger than 2 ( $\xi(2) > 1$ ), can be found at mid latitudes below the auroral oval. As al-  
 388 ready underlined in the previous Section, looking at the spatial distribution of the strongest  
 389 and most pronounced irregularities, i.e. of the highest values of RODI, we remark that  
 390 they are essentially oriented in the day–night direction across the polar cap. These ir-  
 391 regularities could be mainly attributed to dynamical processes including high-speed plasma  
 392 convection (*Cherniak and Zakharenkova, 2016*). This suggests that the turbulent nature  
 393 of the electron density fluctuations can be due to a Kelvin–Helmholtz instability and/or  
 394 gradient-drift instability in those regions characterized by strong shear flows. Now, for  
 395 low- $\beta$  plasmas (here  $\beta = p_k/p_B$  refers to the ratio between kinetic plasma pressure  $p_k$   
 396 and magnetic pressure  $p_B$ ) the expected turbulence is 2D and mainly fluid, generated  
 397 by electrostatic fluctuations and characterized by a near -5/3 power spectral density, but  
 398 the energy cascade is backward in the low frequency range (*Kintner and Seyler, 1985*).  
 399 In this framework, shear-flow associated instabilities are the principal mechanism to gen-  
 400 erated turbulent fluctuations. However, we cannot exclude that the auroral particle pre-  
 401 cipitation could also be another source of the observed turbulent behavior mainly in the  
 402 Northern Hemisphere where the high values of RODI tend to be concentrated along the  
 403 auroral oval border. Looking at the values of the second-order scaling exponent  $\xi(2)$  as-  
 404 sociated with the second RODI family at values  $< 3 \times 10^3 \text{ cm}^{-3} \text{s}^{-1}$  one can note how  
 405 this second family is characterized by  $\xi(2) > 1$  (i.e., spectral scaling exponents higher  
 406 than 2). These values are generally spatially located outer of the border of the convec-  
 407 tion zone, where different physical mechanisms could be responsible for the observed scal-  
 408 ing features.

409 For more detailed study of the spatial distribution of the strongest and most pro-  
 410 nounced irregularities during this geomagnetic storm, in the context of two-cell plasma  
 411 convection, we compared RODI maps with Super Dual Auroral Radar Network (Super-  
 412 DARN) polar potential maps obtained using the statistical convection model CS10 (*Cousins*  
 413 *and Shepherd, 2010*). In this model high-latitude ionospheric convection patterns are  
 414 obtained using average convection patterns derived from the SuperDARN measurements  
 415 collected over many years for varying solar wind velocity, interplanetary magnetic field  
 416 and dipole tilt angle conditions. We have evaluated, for each day, the average values of  
 417 these parameters and derived the corresponding average convection patterns indepen-  
 418 dently for the Northern Hemisphere and Southern Hemisphere. Of course, these are av-  
 419 erage daily patterns which do not describe the real convection patterns characterizing  
 420 the analyzed regions. The latter may indeed drastically change with varying interplan-  
 421 etary conditions. The average convection pattern, however, allows to understand where  
 422 the irregularities described by the RODI are distributed.

423 Figure 5 reports a comparison between RODI and SuperDARN polar potential maps  
 424 obtained using the statistical convection model CS10. Figure 5 reports the results ob-  
 425 tained in both hemispheres in two different days, 17 and 19 March 2015, respectively.  
 426 As we have hypothesized looking at the spatial distribution of the RODI values, the strongest

427 and most pronounced irregularities during the geomagnetically disturbed days seem to  
428 follow the convection patterns. They are mainly localized along the convection patterns  
429 that travel across the polar cap from the dayside to the nightside. This result seems to  
430 support our hypothesis according to which the physical mechanisms responsible for the  
431 formation of high-latitude ionospheric irregularities characterized by high values of RODI  
432 can be both the gradient-drift and the Kelvin–Helmholtz instability, while perhaps the  
433 low RODI values’ family could be due to a different kind of turbulent/stochastic pro-  
434 cess.

## 435 5 Conclusions

436 The high-latitude ionosphere is extremely rich in plasma irregularities and fluctu-  
437 ations. They are due to a very long list of processes which depend mainly on the scale  
438 of interest. In the spatial scales from hundreds of kilometers down to some kilometers  
439 these irregularities partially depend on the interaction of the high-ionosphere with the  
440 various magnetospheric regions to which it is connected by magnetic field lines (*Kelley*,  
441 2009). Over the past two decades several studies focused on the characterization of plasma  
442 density irregularities and fluctuations at different spatial scales by using both ground-  
443 based observations and in situ measurements on-board LEO satellites. Our work has to  
444 be placed within this framework.

445 We have studied the nature of electron density fluctuations recorded on-board Swarm  
446 satellites at mid- and high-latitude regions in both hemispheres in order to investigate  
447 the self-similarity/affinity nature of the measured time series. We have thus looked for  
448 scaling invariance in the plasma density fluctuations (in terms of self-similarity) support-  
449 ing the idea that turbulence might play a role in generating plasma irregularities. Based  
450 on this idea we have investigated a possible link between the observed scaling features  
451 and the electron density irregularities identified by RODI. Among the different irregu-  
452 larity parameters that can be derived from the plasma density measurements, RODI is  
453 indeed a measure of the electron density variations that shows a high correlation degree  
454 with the pattern of topside ionospheric irregularities (*Zakharenkova et al.*, 2016).

455 So, the joint analysis of RODI and of the scaling features of electron density fluctu-  
456 ations recorded by Swarm A and B gave us the opportunity to locally analyze the small-  
457 scale (both spatial and temporal) fluctuations of electron density and investigate a pos-  
458 sible relation between their properties and RODI in the ionospheric topside region. The  
459 study highlighted two families of plasma irregularities that seem to be associated with  
460 different physical properties. On one hand, there are plasma density variations associ-  
461 ated with low values of RODI that are characterized by scaling properties not support-  
462 ing the idea of a fluid and/or MHD turbulence as a source of these perturbations. These  
463 irregularities mainly occur in the mid-latitude regions mainly below the auroral oval. On  
464 the other hand, there are plasma density variations associated with high RODI values  
465 ( $> 10^{3.5} \text{ cm}^{-3} \text{ s}^{-1}$ ) and scale-invariant anti-persistent fluctuations that are character-  
466 ized by spectral properties similar to those expected in the case of fluid and/or MHD  
467 turbulence. Indeed, in this case, the second-order scaling exponent to which the spec-  
468 tral feature is related, ranges from 0.5 to 0.8, supporting a near 5/3 spectral features (a  
469 quasi-Kolmogorov scaling) of the observed density fluctuations. These irregularities mainly  
470 occur at high latitudes in the auroral and polar cap regions and can be caused by direct  
471 particle precipitation and by dynamic plasma processes in the polar ionosphere involv-  
472 ing turbulence. In other words they could be associated with a fluid/MHD plasma tur-  
473 bulence mechanisms generated by Kelvin-Helmholtz or shear-flow instabilities. We note  
474 how the location of these irregularities seems to be associated with the convection pat-  
475 tern, i.e., with the plasma transport across the polar cap as recently observed (*Yang et*  
476 *al.*, 2016). Conversely, the second family of RODI values could be the consequence of a  
477 different turbulent and/or stochastic mechanism.

Our observations suggest that RODI, which is a proxy of ionospheric irregularities, cannot be generically considered as a proxy of the occurrence of ionospheric fluid/MHD turbulence. It is nevertheless true that its highest values ( $> 10^{3.5} \text{ cm}^{-3} \text{ s}^{-1}$ ) can give us information on the possible turbulent origin of the plasma irregularities. However, we cannot exclude that different turbulent/stochastic mechanism could be responsible for the occurrence of scaling (self-similar) features also in the case of RODI small values. This point deserves a more detailed analysis which calls for future work.

### Acknowledgments

The results presented rely on data collected by two of the three satellites of the Swarm constellation. We thank the European Space Agency (ESA) that supports the Swarm mission. Swarm data can be accessed at <http://earth.esa.int/swarm>. The authors kindly acknowledge V. Papitashvili and J. King at the National Space Science Data Center of the Goddard Space Flight Center for the use permission of 1 min OMNI data and the NASA CDAWeb team for making these data available (<https://cdaweb.gsfc.nasa.gov/index.html/>). The authors acknowledge financial support from European Space Agency (ESA contract N. 4000125663/18/I-NB- "EO Science for Society Permanently Open Call for Proposals EOEP-5 BLOCK4 (INTENS)).

### References

- Alessio E., A. Carbone, G. Castelli, and V. Frappietro (2002), Second-order moving average and scaling of stochastic time series, *Eur. Phys. J. B*, 27, 197-200.
- Astafyeva, E., I. Zakharenkova, and M. Förster (2015), Ionospheric response to the 2015 St. Patrick's day storm: A global multi-instrumental overview, *J. Geophys. Res.*, 120, 9023–9037, doi:10.1002/2015JA021629.
- Balasis G., I. A. Daglis, P. Kapiris, M. Manda, D. Vassiliadis, and K. Eftaxias (2006), From pre-storm activity to magnetic storms: a transition described in terms of fractal dynamics, *Ann. Geophys.*, 24, 3557-3567.
- Balasis, G., Daglis, I. A., Contoyiannis, Y., Potirakis, S. M., Papadimitriou, C., Melis, N. S., et al. (2018). Observation of intermittency-induced critical dynamics in geomagnetic field time series prior to the intense magnetic storms of March, June, and December 2015. *Journal of Geophysical Research: Space Physics*, 123, 4594–4613, doi:10.1002/2017JA025131.
- Basu S., S. Basu, E. MacKenzie, W. R. Coley, W. B. Hanson and C. S. Lin (1984), F-region electron density irregularity spectra near auroral acceleration and shear regions, *J. Geophys. Res.*, 89, 5554.
- Basu S., S. Basu, E. MacKenzie, P. F. Fougere, W. R. Coley, N. C. Maynard, J. D. Winningham, M. Sugiura, W. B. Hanson, and W. R. Hoegy (1988), Simultaneous density and electric field fluctuation spectra associated with velocity shears in the auroral oval, *J. Geophys. Res.*, 93, 115.
- Carbone A., G. Castelli, and H. E. Stanley (2004), Time-dependent Hurst exponent in financial time series, *Physica A*, 344, 267-271.
- Cousins, E. D. P., and S. G. Shepherd (2010), A dynamical model of high-latitude convection derived from SuperDARN plasma drift measurements, *J. Geophys. Res.*, 115, A12329, doi:10.1029/2010JA016017.
- Cerisier J. C., J. J. Berthelier and C. Beghin (1985), Unstable density gradients in the high-latitude ionosphere, *Radio Sci.*, 20, 755.
- Chaston C.C., et al. (2008) The turbulent Alfvénic aurora, *Phys. Rev. Lett.*, 100, 175003.
- Cherniak, I., I. Zakharenkova, and R. J. Redmon (2015), Dynamics of the high-latitude ionospheric irregularities during the 17 March 2015 St. Patrick's Day storm: Ground-based GPS measurements, *Space Weather*, 13, 585–597, doi:10.1002/2015SW001237.

- 529 Cherniak and Zakharenkova (2016) High-latitude ionospheric irregularities: differ-  
 530 ences between ground- and space-based GPS measurements during the 2015  
 531 St. Patrick's Day storm Earth, Planets and Space 68,136 DOI 10.1186/s40623-  
 532 016-0506-1
- 533 De Michelis P., G. Consolini, and R. Tozzi (2015), Magnetic field fluctuation features  
 534 at Swarm's altitude: A fractal approach, *Geophys. Res. Lett.*, 42, 31003105,  
 535 doi:10.1002/2015GL063603.
- 536 De Michelis P., G. Consolini, R. Tozzi, and M. F. Marcucci (2017), Scaling features  
 537 of high latitude geomagnetic field fluctuations at Swarm altitude: Impact of  
 538 IMF orientation, *J. Geophys. Res. Space Phys.*, doi:10.1002/2017JA024156.
- 539 Dyrud L. , B. Krane, M. Oppenheim, H. L. Pécseli, J. Trulsen, and A. W. Wernik  
 540 (2008), Structure functions and intermittency in the ionosphere plasma, *Non-  
 541 lin. Processes Geophys.*, 15, 847.
- 542 Dyson P.L., J. P. McClure W. B. Hanson (1974), In situ measurements of the spec-  
 543 tral characteristics of F region ionospheric irregularities, *J. Geophys. Res.*, 79,  
 544 1497, 1974.
- 545 Earle G. D. , M. C. Kelley, and G. Ganguli (1989), Large velocity shears and asso-  
 546 ciated electrostatic waves and turbulence in the auroral F region, *J. Geophys.  
 547 Res.*, 94, 15,321, doi:10.1029/JA094iA11p15321.
- 548 Giannattasio F., P. De Michelis, G. Consolini, V. Quattrociochi, I. Coco, and R.  
 549 Tozzi (2019), Characterising the electron density fluctuations in the high-  
 550 latitude ionosphere at Swarm altitude in response to the geomagnetic activity,  
 551 *Annals of Geophysics*, 61, doi:10.4401/ag-7716.
- 552 Gjerloev, J. W., Ohtani, S., Iijima, T., Anderson, B., Slavin, J., and Le, G. (2011),  
 553 Characteristics of the terrestrial field-aligned current system, *Ann. Geophys.*,  
 554 29, 1713-1729.
- 555 Golovchanskaya I. V., A. A. Ostapenko, and B. V. Kozelov (2006), Relation-  
 556 ship between the high-latitude electric and magnetic turbulence and  
 557 the Birkeland field-aligned currents, *J. Geophys. Res.*, 111, A12301,  
 558 doi:10.1029/2006JA011835.
- 559 Golovchanskaya I. V. , and B. V. Kozelov (2010), On the origin of electric  
 560 turbulence in the polar cap ionosphere, *J. Geophys. Res.*, 115, A09321,  
 561 doi:10.1029/2009JA014632.
- 562 Grach S. M. , E .N. Sergeev, E. V. Mishin, and A. V. Shindin (2016), Dynamic  
 563 properties of ionospheric plasma turbulence driven by high-power high-  
 564 frequency radiowaves, *Phys. Usp.*, 59, 1091.
- 565 Heppner J. P., M. C. Liebrecht, N. C. Maynard, and R. F. Pfaff (1993), High-  
 566 latitude distributions of plasma waves and spatial irregularities from DE2  
 567 alternating current electric field observations, *J. Geophys. Res.*, 98, 1629.
- 568 Hurst, H. (1956). Methods of using long-term storage in reservoirs. *ICE Proceedings*,  
 569 5(704), 519543.
- 570 Jin, Y., Spicher, A., Xiong, C., Clausen, L. B. N., Kervalishvili, G., Stolle, C.,  
 571 and Miloch, W. J. (2019). Ionospheric plasma irregularities characterized  
 572 by the Swarm satellites: Statistics at high latitudes. *J. Geophys. Res. Space  
 573 Physics*, 124, 1262–1282.
- 574 Kelley M. C. (2009), *The Earth's Ionosphere Plasma Physics and Electrodynamics*,  
 575 2nd ed., Elsevier, Amsterdam.
- 576 Kintner P. M. Jr., and C. E. Seyler (1985), The status of observations and theory  
 577 of high latitude ionosphere and magnetospheric plasma turbulence, *Space Sci.  
 578 Rev.*, 41, 91.
- 579 Kozelov B. V., and I. V. Golovchanskaya (2006), Scaling of electric field fluctuations  
 580 associated with the aurora during northward IMF, *Geophys. Res. Lett.*, 33,  
 581 L20109, doi:10.1029/2006GL027798.
- 582 Knudsen, D. J., J. K. Burchill, S. C. Buchert, A. I. Eriksson, R. Gill, J.-E. Wahlund,  
 583 L. Ahlen, M. Smith, and B. Moffat (2017), Thermal ion imagers and Lang-

- 584 muir probes in the Swarm electric field instruments, *J. Geophys. Res. Space*  
585 *Physics*, 122, 2655–2673, doi:10.1002/2016JA022571.
- 586 Laundal K. M., and Richmond A.D. (2016), *Magnetic Coordinate Systems*, *Space*  
587 *Sci. Rev.*, doi 10.1007/s11214-016-0275-y.
- 588 Mounir H., A. Berthelier, J. C. Cerisier, D. Lagoutte, and C. Beghin (1991), The  
589 small-scale turbulent structure of the high latitude ionosphere-Arcad-Aureol-3  
590 observations, *Annales Geophysicae*, 9, 725.
- 591 Nava, B., J. Rodríguez-Zuluaga, K. Alazo-Cuartas, A. Kashcheyev, Y. Migoya-Oruè,  
592 S. M. Radicella, C. Amory-Mazaudier, and R. Fleury (2016), Middle- and low-  
593 latitude ionosphere response to 2015 St. Patrick's Day geomagnetic storm, *J.*  
594 *Geophys. Res. Space Physics*, 121, 3421–3438, doi:10.1002/2015JA022299.
- 595 Olsen, N., Friis-Christensen, E., Floberghagen, R. et al. (2013), The Swarm Satellite  
596 Constellation Application and Research Facility (SCARF) and Swarm data  
597 products, *Earth Planet Sp* 65: 1.
- 598 Pécseli H. (2016), Turbulence in the ionosphere, Chapter 24 of “Low Frequency  
599 Waves and Turbulence in Magnetized Laboratory Plasmas and in the Iono-  
600 sphere” by H. Pécseli edit by IOP Science.
- 601 Peng C. K., Buldyrev S. V., Havlin S., Simons M., Stanley H. E., Goldberger A.  
602 L. (1994), Mosaic organization of DNA nucleotides. *Phys. Rev. E Stat. Phys.*  
603 *Plasmas Fluids Relat. Interdiscip. Topics* 49, 1685.
- 604 Poppe, B.B. (2000) New scales help public, technicians understand space weather.  
605 *Eos Trans. AGU*, 81 (29), 322–328, DOI: 10.1029/00EO00247.
- 606 Pröls, G. W. (1987), Storm-induced changes in the thermospheric composition at  
607 middle latitudes, *Planetary and Space Science*, 35, 807–811, doi:10.1016/0032-  
608 0633(87)90041-9.
- 609 Ram, S. T., T. Yokoyama, Y. Otsuka, K. Shiokawa, S. Sripathi, B. Veenadhari, R.  
610 Heelis, K. K. Ajith, V. S. Gowtam, S. Gurubaran, P. Supnithi, and M. L. Huy  
611 (2015), Duskside enhancement of equatorial zonal electric field response to  
612 convection electric fields during the St. Patrick's day storm on 17 march 2015,  
613 *J. Geophys. Res.*, doi: 10.1002/2015JA021932.
- 614 Ramsingh, S. Sripathi, S. Sreekumar, S. Banola, K. Emperumal, P. Tiwari, and  
615 B. S. Kumar (2015), Low-latitude ionosphere response to super geomag-  
616 netic storm of 17/18 March 2015: Results from a chain of ground-based  
617 observations over indian sector, *J. Geophys. Res.*, 120, 10,864–10,882,  
618 doi:10.1002/2015JA021509.
- 619 Spicher A., W. J. Miloch, L. B. N. Clausen and J. I. Moen (2015), Plasma  
620 turbulence and coherent structures in the polar cap observed by the  
621 ICI-2 sounding rocket, *J. Geophys. Res. Space Physics*, 120, 110,978,  
622 doi:10.1002/2015JA021634.
- 623 Tam S., W. Y. Chang, P. M. Kintner, and E. Klatt (2005), Intermittency Analy-  
624 ses on the SIERRA Measurements of the Electric Field Fluctuations in the  
625 Auroral Zone, *Geophys. Res. Lett.*, 32, L05109.
- 626 Weimer D. R., C. K. Goertz, and D. A. Gurnett (1985), Auroral Zone Electric Fields  
627 from DE1 and 2 at Magnetic Conjunctions, *J. Geophys. Res.*, 90A, 7479.
- 628 Wiener N. (1964), *Time Series*. M.I.T. Press, Cambridge, Massachusetts. p. 42.
- 629 Yang S.-G., B.-C. Zhang, H.-X. Fang, Y. Kamide, et al., (2016), New evidence of  
630 dayside plasma transportation over the polar cap to the prevailing dawn sector  
631 in the polar upper atmosphere for solar-maximum winter, *J. Geophys. Res.:*  
632 *Space Phys.*, 121, 5626, DOI 10.1002/2015JA022171.
- 633 Zakharenkova I., E. Astafyeva, and I. Cherniak, (2016), GPS and in situ Swarm  
634 observations of the equatorial plasma density irregularities in the topside iono-  
635 sphere, *Earth, Planets and Space*, 68, 120 DOI 10.1186/s40623-016-0490-5.

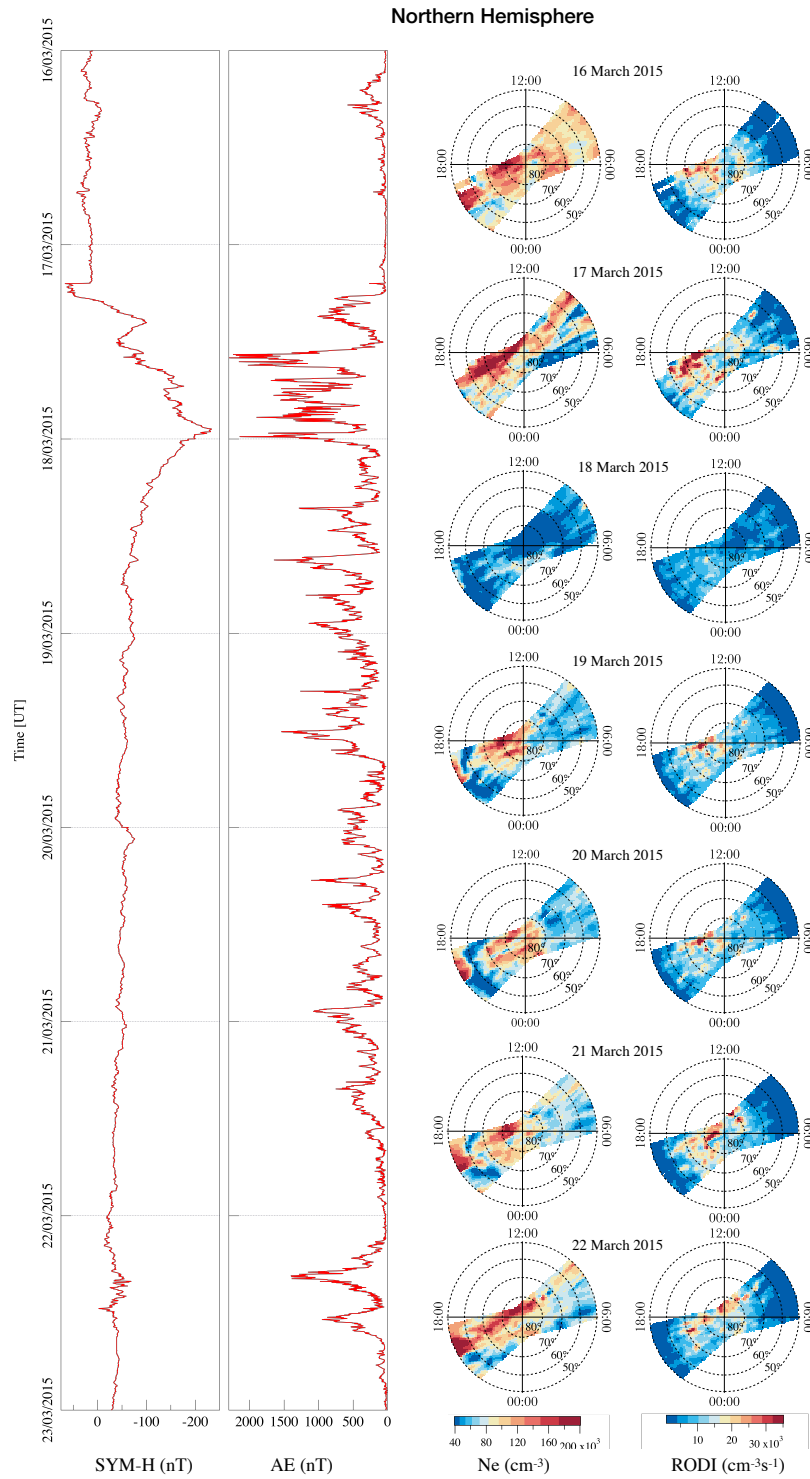


**Figure 1.** Daily maps of the electron density and RODI in the Northern Hemisphere during the selected time interval (16-22 March 2015) for Swarm A and B. Maps are in QD-latitude and MLT coordinate system. In each map, magnetic noon is at the top and magnetic midnight is at the bottom. The concentric circles represent contours of magnetic latitude, separated by intervals of  $10^\circ$ . The two panels on the left report corresponding values of geomagnetic indices SYM-H and AE.

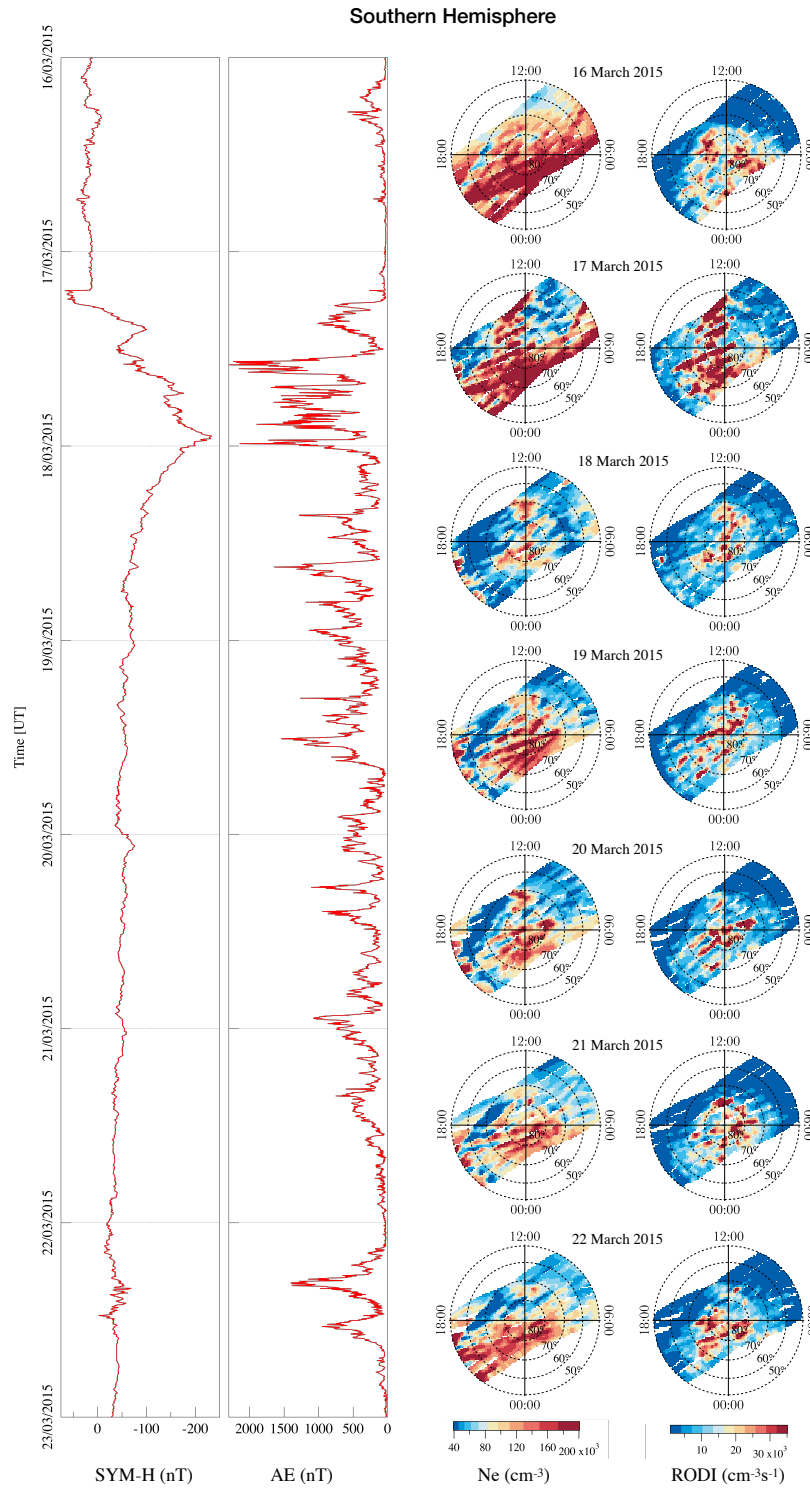


**Figure 2.** Daily maps of the electron density and RODI in the Southern Hemisphere during the selected time interval (16-22 March 2015) for Swarm A and B. Maps are in QD-latitude and MLT coordinate system. In each map, magnetic noon is at the top and magnetic midnight is at the bottom. The concentric circles represent contours of magnetic latitude, separated by intervals of  $10^\circ$ . The two panels on the left report corresponding values of geomagnetic indices SYM-H and AE.

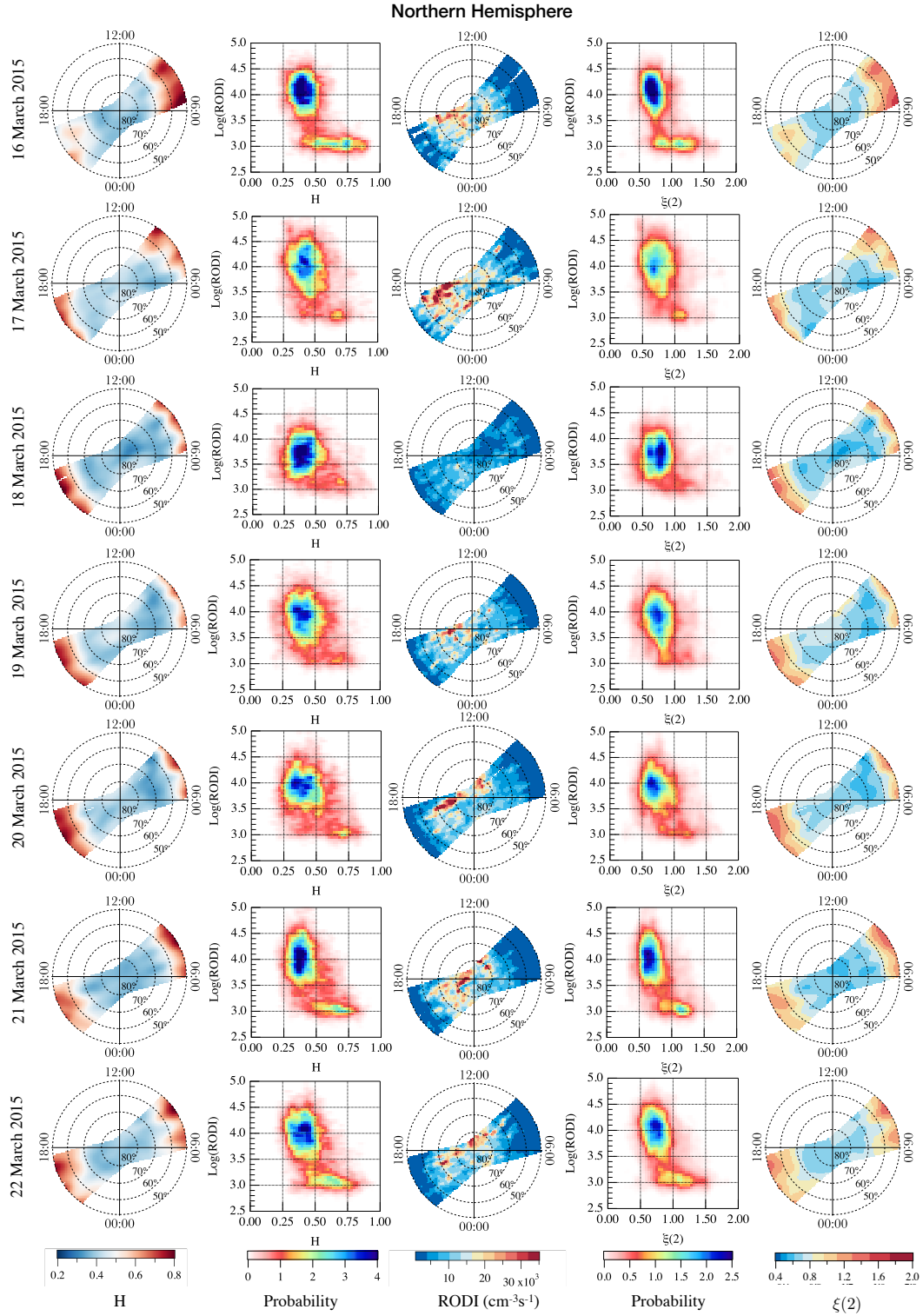


**Figure 3.** From the left daily maps of: 1<sup>st</sup> order scaling exponent, joint probability distribution between the 1<sup>th</sup> order scaling exponent and RODI, RODI, joint probability distribution between the 2<sup>nd</sup> order scaling exponent and RODI and the 2<sup>nd</sup> order scaling exponent. These daily maps cover the time interval 16-22 March 2015 (from top to bottom) in the Northern Hemisphere and are in QD-latitude and MLT coordinate system.



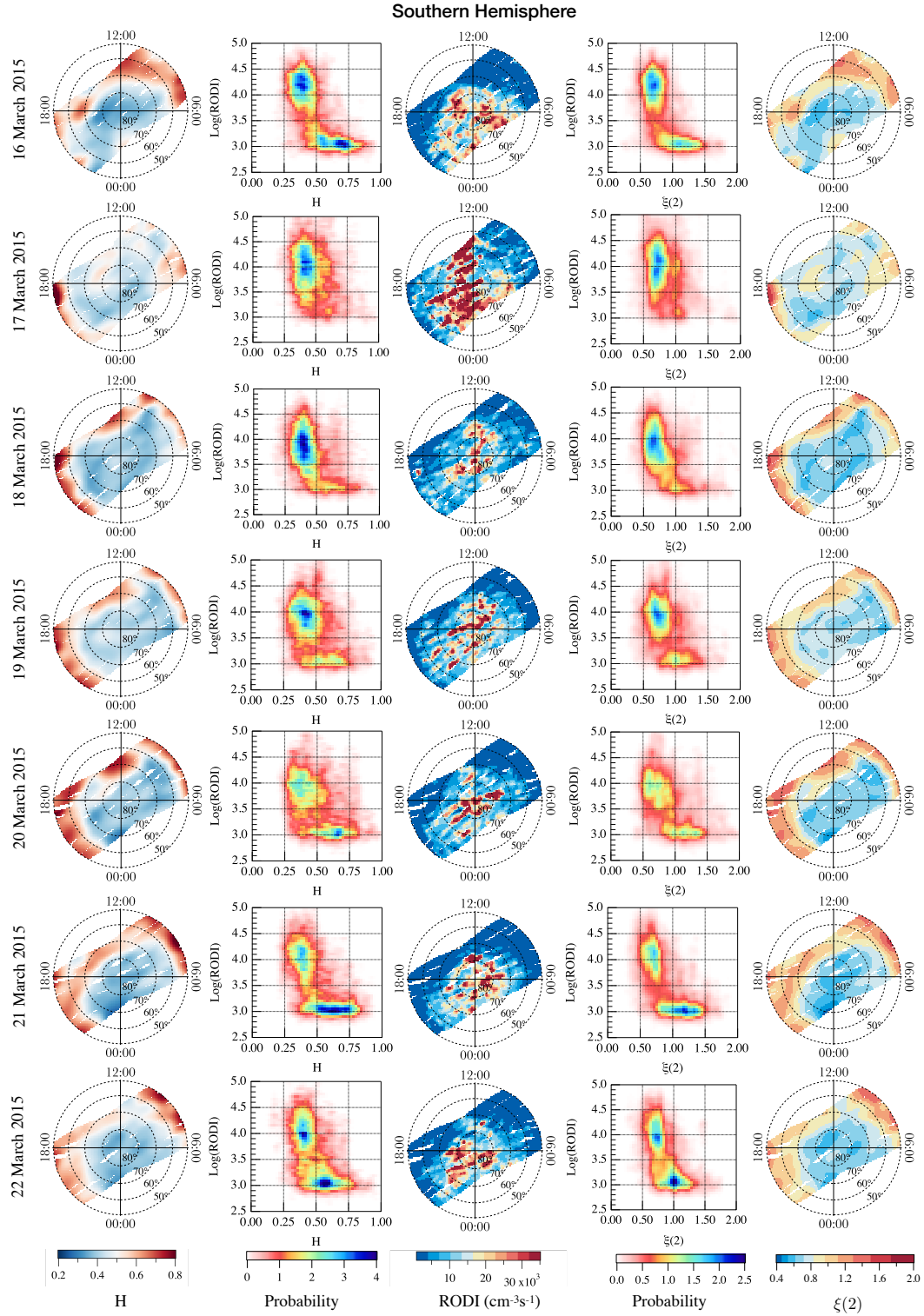


**Figure 4.** From the left daily maps of: 1<sup>st</sup> order scaling exponent, joint probability distribution between the 1<sup>th</sup> order scaling exponent and RODI, RODI, joint probability distribution between the 2<sup>nd</sup> order scaling exponent and RODI and the 2<sup>nd</sup> order scaling exponent. These daily maps cover the time interval 16-22 March 2015 (from top to bottom) in the Southern Hemisphere and are in QD-latitude and MLT coordinate system.

Accepted Article

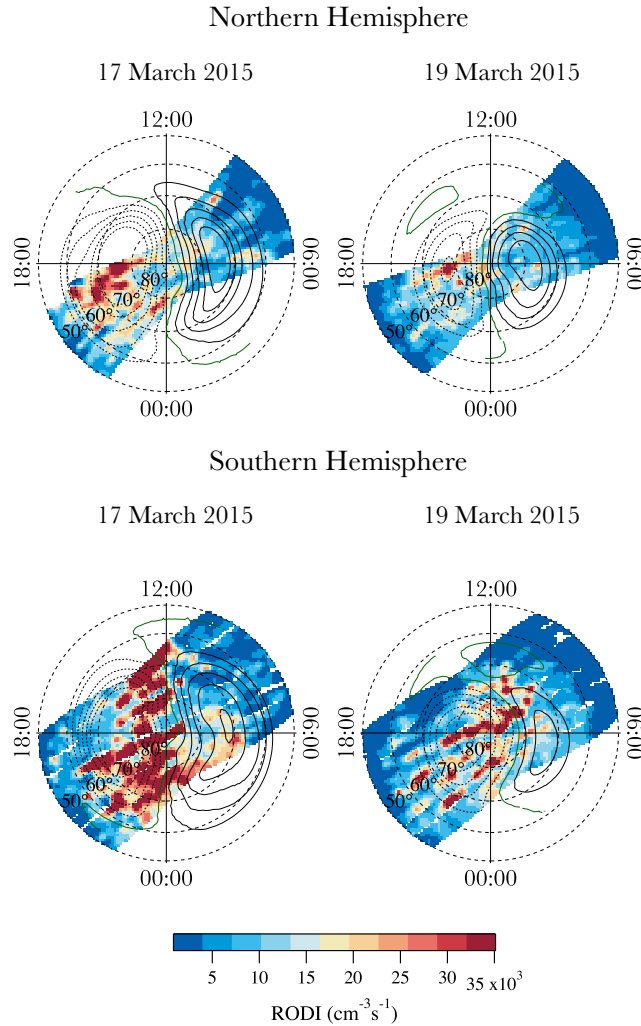


**Figure 5.** An example of comparison between satellite observations of RODI with SuperDARN polar potential maps obtained using the statistical convection model CS10. Data are reported as a function of MLT and QD latitude for two specific days for the Northern and Southern Hemispheres. The concentric circles represent contours of magnetic latitude, separated by intervals of  $10^\circ$ . The black contours are the ionospheric potential pattern, at 10 kV intervals. The dashed lines refer to negative values while the continuous lines to the positive ones.